

One-loop corrections to the Drell–Yan process in SANC

(II) The neutral current case.

A. Arbuzov^{1,2} e-mail: arbuzov@theor.jinr.ru, D. Bardin², S. Bondarenko^{1,2}, P. Christova²,
L. Kalinovskaya², G. Nanava^{3a}, and R. Sadykov²

¹ Bogoliubov Laboratory of Theoretical Physics,
JINR, Dubna, 141980 Russia

² Dzhelepov Laboratory of Nuclear Problems,
JINR, Dubna, 141980 Russia

³ IFJ, PAN, Krakow, 313-42 Poland

the date of receipt and acceptance should be inserted later

Abstract. Radiative corrections to the neutral current Drell–Yan-like processes are considered. Complete one-loop electroweak corrections are calculated within the SANC system. Theoretical uncertainties are discussed. Numerical results are presented for typical conditions of LHC experiments.

Key words. Drell–Yan process – electroweak radiative corrections

PACS. 1 3.85.Qk Inclusive production with identified leptons, photons, or other nonhadronic particles; 12.15.Lk Electroweak radiative corrections

^a on leave from IHEP, TSU, Tbilisi, Georgia

1 Introduction

The current theoretical status of Drell–Yan [1] physics is widely overviewed in the recent papers [2, 3] where the necessity of further in-depth study of the Drell–Yan-like (DY) processes is emphasized.

At hadron–hadron colliders DY processes serve for the normalization purposes [4, 5], provide information about weak interactions [6, 7], contribute to the background in many searches for new physics beyond the Standard Model (SM). At the LHC they will be used also for precision fits of partonic density functions in the regions of x and factorization scale values which were not yet accessed experimentally.

The theoretical calculations of the DY processes for high energy hadronic colliders were performed at the level of one-loop QED and electroweak (EW) radiative corrections (RC) by several groups, see papers [8–17] and references therein. QCD corrections are known up to the next-to-next-to-leading order [18–20].

For the experiment, both charge current (CC) and neutral current (NC) DY processes represent great interest. Both types of the processes can be easily detected. CC processes have a larger cross section, but NC processes have a clean dimuon signature and provide an additional information, *e.g.* about the weak mixing angle.

The theoretical study for CC DY is pushed ahead more than for NC — several independent codes exist for EW NLO RC, see [3]. Within the 2005 Les Houches workshop [21] and the 2006 TEV4LHC workshop [22]

a tuned comparison at partonic and hadronic levels at one-loop precision was realized between four codes: [12], [15], [16] and [23, 24].

To the contrary, a detailed tuned comparison for neutral current DY NLO either at parton or at hadron levels is still on the way. In Ref. [25] one can find a comparison between the results of the HORACE and ZGRADE codes for the inclusive NC DY cross section at the hadronic level. Partial results of the comparison at the partonic level between SANC and another code can be found in [26].

This article is the second step in the series of SANC papers devoted to DY processes. First, we presented in Ref. [27] the CC case. Here we show results for the NC case. Moreover, in the DY branches of SANC we can study the interplay between QCD and EW NLO corrections within the same framework. The current status of this study was presented in the report to ATLAS MC working group at CERN [28]. Detailed description of the QCD branch for DY CC and NC processes will be presented elsewhere, though the first results are already published in [29].

The paper is organized as follows. In the second section we demonstrate the implementation of the EW NLO corrections into the SANC framework [23]. The location of the standard set of the SANC modules: **FF** (form factors), **HA** (helicity amplitudes), **BR** and **MC** (bremsstrahlung), is shown on the screenshot of the **SANC Processes** in the **EW 4f NC** sector. *Ibidem* we show the rather short analytical expression

for the differential cross section of the hard photon contribution.

SANC team has the advantage of experience in the calculation of bremsstrahlung. We can obtain the numerical results both by the semi-analytical expressions (it is the standard **BR** module of the SANC) and by a Monte Carlo integrator or generator (with help of the new **MC** module).

In the third section we describe the adopted “subtraction” procedure in the expressions for virtual, soft and hard contributions to the NC DY cross section.

Numerical results are presented in the Sect. 4 both for the Born and for the EW NLO RC. We investigated the independence of the result on the variation of the soft-hard separator $\bar{\omega}$ which provides one of the most important checks of the calculation. The sensitivity of the corrections to the variation of “subtracted” quark mass singularities was also studied.

In the conclusion we overview the present status of implementation of NC DY calculations into the SANC system.

As the main point of this article we offer for the import a stand-alone code for NC DY EW NLO RC at the partonic level together with the environment in which it was run. The sketchy description of this code is presented in Appendix. Codes are accessible from SANC project homepages <http://sanc.jinr.ru> and <http://pcphsanc.cern.ch>.

For production of numbers at the hadronic level the SANC team created a Monte Carlo integrator and

an event generator, based on the FOAM package [30].

The generator itself will be described elsewhere (see [31])

and made accessible from the project homepages after intensive rolling and testing.

2 Neutral current Drell–Yan processes

2.1 Born level

At first we will consider interactions of *free* quarks (partons). At the leading order (LO) the unpolarized cross section of the partonic subprocess $\bar{q}(p_1)+q(p_2) \rightarrow (\gamma, Z) \rightarrow \ell(p_3) + \bar{\ell}(p_4)$, $q = (u, d, c, s, b)$ is given by

$$\hat{\sigma}_0(\hat{s}) = \frac{4\pi\alpha^2}{9\hat{s}} \beta_{\hat{s}} \left[\left(1 - \frac{m_{\ell}^2}{\hat{s}}\right) V_0(\hat{s}) + \frac{3m_{\ell}^2}{\hat{s}} V_A(\hat{s}) \right], \quad (1)$$

where

$$\begin{aligned} \hat{s} &= -(p_1 + p_2)^2, \\ \beta_{\hat{s}} &= \sqrt{1 - \frac{4m_{\ell}^2}{\hat{s}}}, \end{aligned} \quad (2)$$

and m_{ℓ} being the lepton mass. Here we denoted

$$\begin{aligned} V_{0,A}(\hat{s}) &= Q_q^2 Q_{\ell}^2 + 2Q_q Q_{\ell} v_q v_{\ell} \text{Re}\chi(\hat{s}) \\ &+ (v_q^2 + a_q^2) (v_{\ell}^2 \pm a_{\ell}^2) |\chi(\hat{s})|^2, \\ v_q &= I_q^{(3)} - 2Q_q \sin^2 \theta_W, \\ v_{\ell} &= I_{\ell}^{(3)} - 2Q_{\ell} \sin^2 \theta_W, \\ a_q &= I_q^{(3)}, \\ a_{\ell} &= I_{\ell}^{(3)}. \end{aligned} \quad (3)$$

The Z/γ propagator ratio $\chi_Z(\hat{s})$ with constant (or \hat{s} -dependent) Z width reads

$$\chi_Z(\hat{s}) = \frac{1}{4s_W^2 c_W^2} \frac{\hat{s}}{\hat{s} - M_Z^2 + iM_Z \Gamma_Z}, \quad (4)$$

where s_W and c_W are the sine and cosine of the weak mixing angle θ_W .

2.2 EW Radiative Corrections at the Partonic Level

As the rule of the SANC basement, we subdivide the EW RC into the virtual (loop) ones, the ones due to soft photon emission, and the ones due to hard photon emission. Later on in the section 4 in the Tables 1 and 2, we demonstrate the independence of the EW RC off an auxiliary parameter $\bar{\omega}$ which subdivides the soft and hard photonic contributions.

In Fig. 1 we show the location of the $2f \rightarrow 2f$ NC processes at the SANC tree.

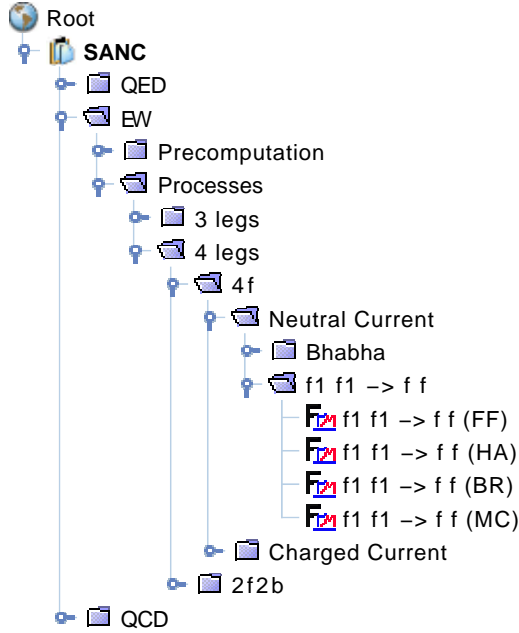


Fig. 1. SANC tree for the process $2f \rightarrow 2f$

Moving along the menu sequence **SANC** \rightarrow **EW** \rightarrow **Processes** \rightarrow **4 legs** \rightarrow **4f** \rightarrow **Neutral Current** \rightarrow **f1 f1** \rightarrow **f f (FF,HA,BR,MC)** user arrives at the first standard SANC module, the scalar Form Factors (FF); then at the second module, Helicity Amplitudes (HA); then at the third module, the integrated

bremsstrahlung (BR); and finally at the fourth module, the fully differential bremsstrahlung (MC).

- FF and HA

Earlier, in our article [23] we presented the Covariant (CA) and Helicity Amplitudes (HA) of $f_1 \bar{f}_1 f \bar{f} \rightarrow 0$ NC process, with all 4-momenta being incoming, for any of its cross channels s, t or u . The expressions for the CA and HA (see Eq.(30) and (33) of the last reference) of this process can be written in terms of six FF.

- BR and MC

The BR module computes the soft and inclusive hard real photon emission:

$$\bar{q}(p_1) + q(p_2) \rightarrow \ell(p_3) + \bar{\ell}(p_4) + \gamma(p_5), \quad (5)$$

where the momenta of corresponding particles are given in brackets. We do not discuss the soft photon contribution here, referring the reader to the system itself. As far as hard photons are concerned, we realized two possibilities of the integration over its phase space: the semi-analytical one (BR) and the one by means of a Monte Carlo integrator or generator (MC).

The first one is based on two different sets of analytical integrals over two choices of kinematic variables parametrizing the hard photon phase space. In the first option (CalcScheme=0), the phase space looks like

$$d\Phi^{(3)} = d\Phi_1^{(2)} d\Phi_2^{(2)} \frac{d\hat{s}'}{2\pi}, \quad (6)$$

where the two-body phase spaces are:

$$d\Phi_1^{(1)} = \frac{1}{8\pi} \frac{\sqrt{\lambda(\hat{s}, \hat{s}', 0)}}{\hat{s}} \frac{1}{2} d\cos\theta_\gamma,$$

$$d\Phi_2^{(2)} = \frac{1}{8\pi} \frac{\sqrt{\lambda(\hat{s}', m_\ell^2, m_\ell^2)}}{\hat{s}'} \frac{1}{4\pi} d\cos\theta_3 d\phi_3. \quad (7)$$

Here, $\hat{s}' = -(p_3 + p_4)^2$ and θ_γ is the cms angle of the photon. Since, for the chosen parametrization of the phase-space the process matrix element squared does not depend on the angle ϕ_γ – cms azimuthal angle of the photon – it is already integrated out in the phase-space. The angles θ_3 and ϕ_3 define the orientation of the momentum p_3 in the rest frame of the compound ($\mathbf{p}_3 + \mathbf{p}_4 = 0$). These parameters vary in the limits:

$$\begin{aligned} 0 \leq \theta_\gamma, \theta_3 \leq \pi, \quad 0 \leq \phi_3 \leq 2\pi, \\ 4m_\ell^2 \leq \hat{s}' \leq \hat{s} - 2\sqrt{\hat{s}}\bar{\omega}. \end{aligned} \quad (8)$$

After the integration over all angular variables, we obtained the compact expression for a single differential distribution of the hard photon contribution to the NC DY process, $d\hat{\sigma}_{\text{hard}}/d\hat{s}'$. We neglected terms proportional to the initial quark mass but kept terms proportional to the lepton mass:

$$\begin{aligned} \frac{d\hat{\sigma}_{\text{hard}}}{d\hat{s}'} &= \frac{\alpha}{\pi} \frac{\hat{s}^2 + \hat{s}'^2}{\hat{s}^2 \hat{s}_-} \left[Q_q^2 \left(\ln \frac{\hat{s}}{m_q^2} - 1 \right) \hat{\sigma}_0(\hat{s}') \right. \\ &+ Q_\ell^2 (L'_\beta - \beta_{\hat{s}'}) \frac{1}{\beta_{\hat{s}}} \hat{\sigma}_0(\hat{s}) \Big] \\ &+ \frac{2\alpha^3}{3} Q_q Q_\ell \frac{\hat{s}_+}{\hat{s}^3} \left[A_2(\hat{s}, \hat{s}') \left(\frac{m_\ell^2 \hat{s}_+}{\hat{s}'} L'_\beta - \frac{\hat{s}}{\hat{s}_-} \beta_{\hat{s}'} \right) \right. \\ &+ Q_q Q_\ell A_1(\hat{s}, \hat{s}') \frac{m_\ell^2}{\hat{s}'} L'_\beta \Big] \\ &+ \frac{4\alpha^3}{9} Q_\ell^2 \frac{m_\ell^2}{\hat{s}^3} \\ &\times \left\{ V_0(\hat{s}) \left[2 \left(\frac{\hat{s}_-}{\hat{s}} - 2 \frac{\hat{s} - m_\ell^2}{\hat{s}_-} \right) L'_\beta - \frac{\hat{s}_-}{\hat{s}} \beta_{\hat{s}'} \right] \right. \\ &\left. - V_A(\hat{s}) \left[4 \left(\frac{\hat{s}_-}{\hat{s}} + 3 \frac{m_\ell^2}{\hat{s}_-} \right) L'_\beta - 3 \frac{\hat{s}_-}{\hat{s}} \beta_{\hat{s}'} \right] \right\}, \end{aligned} \quad (9)$$

where

$$\begin{aligned} L'_\beta &= \ln \frac{1 + \beta_{\hat{s}'}}{1 - \beta_{\hat{s}'}} , \\ \hat{s}_\pm &= \hat{s} \pm \hat{s}', \end{aligned} \quad (10)$$

with the Born cross section given by Eq. (1). The coupling functions are:

$$\begin{aligned} A_1(\hat{s}, \hat{s}') &= 2a_q a_\ell \text{Re}[\chi(\hat{s}') - \chi(\hat{s})] \\ A_2(\hat{s}, \hat{s}') &= 2Q_q Q_\ell a_q a_\ell \text{Re}[\chi(\hat{s}') + \chi(\hat{s})] \\ &+ 8v_q a_q v_\ell a_\ell \text{Re}[\chi(\hat{s}) \chi^*(\hat{s}')]. \end{aligned} \quad (11)$$

We give also a more simple expression neglecting lepton masses. Then all masses remains only in the arguments of logarithms:

$$\begin{aligned} \frac{d\hat{\sigma}_{\text{hard}}}{d\hat{s}'} &= \frac{\alpha}{\pi} \frac{1}{\hat{s}_-} \frac{\hat{s}^2 + \hat{s}'^2}{\hat{s}^2} \\ &\times \left[Q_q^2 \left(\ln \frac{\hat{s}}{m_q^2} - 1 \right) \hat{\sigma}_0(\hat{s}') + Q_\ell^2 \left(\ln \frac{\hat{s}'}{m_\ell^2} - 1 \right) \hat{\sigma}_0(\hat{s}) \right] \\ &- \frac{1}{3} \frac{\alpha^3}{\hat{s}^2} \frac{\hat{s}_+}{\hat{s}_-} |Q_q Q_\ell| \text{Re} \left[Q_q Q_\ell (\chi_z(\hat{s}) + \chi_z(\hat{s}')) \right. \\ &\left. + 4 v_q v_\ell \chi_z(\hat{s}) \chi_z^*(\hat{s}') \right], \end{aligned} \quad (12)$$

with $\hat{\sigma}_0(\hat{s})$ being the massless limit of Eq. (1).

In the second option (CalcScheme=1), the module BR computes the distribution: $d\hat{\sigma}_{\text{hard}}/d\hat{c}$, where $\hat{c} = \cos(\angle \mathbf{p}_2 \mathbf{p}_4)$. The phase space in this case reads:

$$d\Phi^{(3)} = \frac{1}{2^9 \pi^4 \hat{s}} d\hat{c} d\hat{s}' dZ_4 d\phi_\gamma, \quad (13)$$

where $Z_4 = -2p_4 p_5$ and ϕ_γ is the cms azimuthal angle of p_5 varying within 2π limits. After integration over ϕ_γ , Z_4 , varying within limits

$$\frac{1}{2} \hat{s}_- (1 - \beta_{\hat{s}}) \leq Z_4 \leq \frac{1}{2} \hat{s}_- (1 + \beta_{\hat{s}}), \quad (14)$$

and \hat{s}' — within the same limits as in Eq. (8), one gets very cumbersome result for the single differential distribution over variable \hat{c} , where one has to neglect terms proportional to all masses keeping them only in the arguments of logarithms. The user may see this re-

sult after corresponding run of the SANC **BR** module with CalcScheme=1.

The **MC** module provides fully differential hard bremsstrahlung contribution to the partonic cross section. The contribution is given in a form suitable for further numerical integration or simulation of events in a Monte Carlo generator.

3 Treatment of quark mass singularities

3.1 Partonic level

To perform the subtraction procedure at the partonic level cross section

$$\hat{\sigma}_1 = \hat{\sigma}_0 + \hat{\sigma}_{\text{SV}} + \hat{\sigma}_{\text{hard}}, \quad (15)$$

we proceed in the same way as in our previous paper on DY CC [27].

The subtracted expression $\Delta\hat{\sigma}^{\overline{\text{MS}}}$ from the complete calculations with massive quarks:

$$\Delta\hat{\sigma}_1^{\overline{\text{MS}}} = \sum_{i=1,2} Q_i^2 \frac{\alpha}{2\pi} \int_{\xi_{\min}}^1 d\xi_i \left[\frac{1+\xi_i^2}{1-\xi_i} \left(\ln \frac{M^2}{m_i^2} - 2 \ln(1-\xi_i) - 1 \right) \right]_+ \hat{\sigma}_0(s\xi_i), \quad (16)$$

where

$$\xi_{\min} = \frac{4m_\ell^2}{s}. \quad (17)$$

Next, Q_i and m_i are the charge and the mass of the given quark; M is the factorization scale; $\hat{\sigma}_0(s\xi_i)$ is the cross section at the partonic level with the reduced value of $s \rightarrow s\xi_i$.

The plus prescription in Eq. (16) can be treated in the following way:

$$\Delta\hat{\sigma}_1^{\overline{\text{MS}}} = \lim_{\bar{\omega} \rightarrow 0} (\Delta\hat{\sigma}_{\text{SV}} + \Delta\hat{\sigma}_{\text{hard}})^{\overline{\text{MS}}}. \quad (18)$$

The first contribution, $\Delta\hat{\sigma}_{\text{SV}}$, related to soft and virtual photonic contributions, is given by

$$\Delta\hat{\sigma}_{\text{SV}} = \frac{\alpha}{\pi} Q_q^2 \left(\ln \frac{M^2}{m_q^2} \ln \frac{4\bar{\omega}^2}{s} - \frac{1}{2} \ln^2 \frac{4\bar{\omega}^2}{s} - \ln \frac{4\bar{\omega}^2}{s} + \frac{3}{2} \ln \frac{M^2}{m_q^2} + 2 \right) \hat{\sigma}_0(s), \quad (19)$$

where we took into account that $m_1 = m_2 = m_q$ and $Q_1^2 = Q_2^2 = Q_q^2$ for the NC case.

The second one, $\Delta\hat{\sigma}_{\text{hard}}$, related to hard photon emission, is

$$\Delta\hat{\sigma}_{\text{hard}} = \frac{\alpha}{\pi} Q_q^2 \int_{\xi_{\min}}^{\xi_{\max}} d\xi \left[\frac{1+\xi^2}{1-\xi} \ln \frac{M^2}{m_q^2} - 2 \ln(1-\xi) - 1 \right] \hat{\sigma}_0(s\xi), \quad (20)$$

where

$$\xi_{\max} = \frac{s - 2\sqrt{s\bar{\omega}}}{s}. \quad (21)$$

Using subtraction procedure, the cross section with $\mathcal{O}(\alpha)$ corrections is given by

$$\hat{\sigma}_1^{\overline{\text{MS}}} = \hat{\sigma}_1 - \Delta\hat{\sigma}_1^{\overline{\text{MS}}}. \quad (22)$$

Then it can be convoluted with PDF's in the usual way. An equivalent subtraction procedure applied at the hadronic level will be discussed right below.

3.2 Hadronic level

The differential cross section of the DY process at the hadronic level can be obtained from the convolution

of the partonic cross section with the quark density functions:

$$\frac{d\sigma_1^{pp \rightarrow l\bar{l}X}(s, c)}{dc} = \sum_{q_1 q_2} \int_0^1 \int_0^1 dx_1 dx_2 \bar{q}_1(x_1, M^2) \times \bar{q}_2(x_2, M^2) \frac{d\hat{\sigma}_1^{q_1 \bar{q}_2 \rightarrow l\bar{l}}(\hat{s}, \hat{c})}{d\hat{c}} \mathcal{J} \Theta(c, x_1, x_2), \quad (23)$$

where the step function $\Theta(c, x_1, x_2)$ defines the phase space domain corresponding to the given event selection procedure. The partonic cross section is taken in the center-of-mass reference frame of the initial quarks, where the cosine of the muon scattering angle \hat{c} is defined. The transformation into the angle c defined in the cms of an initial hadrons involves the Jacobian:

$$\mathcal{J} = \frac{\partial \hat{c}}{\partial c} = \frac{4x_1 x_2}{a^2}, \quad a = x_1 + x_2 - c(x_1 - x_2),$$

$$\hat{c} = 1 - (1 - c) \frac{2x_1}{a}, \quad \hat{s} = s x_1 x_2. \quad (24)$$

The parton densities with *bars* in Eq. (23) mean the ones modified by the subtraction of the quark mass singularities:

$$\bar{q}(x, M^2) = q(x, M^2) - \frac{\alpha}{2\pi} Q_q^2 \int_x^1 \frac{dz}{z} q\left(\frac{x}{z}, M^2\right) \times \left[\frac{1+z^2}{1-z} \left(\ln \frac{M^2}{m_q^2} - 2 \ln(1-z) - 1 \right) \right]_+, \quad (25)$$

where $q(x, M^2)$ can be taken directly from the existing PDF's in the \overline{MS} scheme (see Ref. [10] for the corresponding formula in the DIS scheme). It can be shown analytically, that this procedure is equivalent to the subtraction from the cross section, given by Eq. (22). In the approach with subtraction from PDF's it is easy to keep the completely differential form of the sub-process cross section and therefore to impose

any kind of an experimental cut. When the returning to the Z -resonance is allowed by kinematic cuts, the *natural* choice of the factorization scale is $M^2 = M_Z^2$. For the region of higher invariant masses of the lepton pair, M_{l+l-} , it is better to take $M^2 \sim M_{l+l-}^2$.

4 Numerical Results

The input parameters set is taken the same as used in Ref. [21] (`leshw_input.h`, see Appendix):

$$\begin{aligned} G_F &= 1.16637 \times 10^{-5} \text{ GeV}^{-2}, \\ \alpha(0) &= 1/137.03599911, & \alpha_s &= 0.1187, \\ M_W &= 80.425 \text{ GeV}, & \Gamma_W &= 2.124 \text{ GeV}, \\ M_Z &= 91.1867 \text{ GeV}, & \Gamma_Z &= 2.4952 \text{ GeV}, \\ M_H &= 150 \text{ GeV}, & m_t &= 174.17 \text{ GeV}, \\ m_e &= 0.51099892 \cdot 10^{-3} \text{ GeV}, & m_u &= m_d = 66 \text{ MeV}, \\ m_\mu &= 0.105658369 \text{ GeV}, & m_c &= 1.55 \text{ GeV}, \\ m_s &= 150 \text{ MeV}, \\ m_\tau &= 1.77699 \text{ GeV}, & m_b &= 4.5 \text{ GeV}, \\ |V_{ud}| &= |V_{cs}| = 0.975, & |V_{us}| &= |V_{cd}| = 0.222. \end{aligned} \quad (26)$$

4.1 Partonic level

We begin with a presentation of several numerical results derived at the partonic level, investigating the independence of the results of some unphysical parameters and on the choice of an EW scheme. First, we investigate the independence off the parameter $\bar{\omega}$, and the residual dependence on the initial quark masses

after the procedure of subtraction of quark mass singularities (see section 3) by choosing for quark masses two values: first as in Eq. 26, and the second — ten times lower.

4.1.1 Independence off parameter $\bar{\omega}$ and quark masses

The sum of the “soft” and “hard” photon contributions to the total and differential cross sections should not depend on the soft-hard separator $\bar{\omega}$, which we varied from $10^{-3} \frac{\sqrt{s}}{2}$ GeV to $10^{-5} \frac{\sqrt{s}}{2}$ GeV. We observed that for $\bar{\omega} = 10^{-4} \frac{\sqrt{s}}{2}$ GeV and $\bar{\omega} = 10^{-5} \frac{\sqrt{s}}{2}$ GeV the numbers for the one-loop corrected cross sections $\hat{\sigma}_1$ agree within four digits shown, and therefore we present only one row in the Tables 1 and 2. For the relative radiative correction factors there is a tiny dependence on $\bar{\omega}$, and we present the RC for both $\bar{\omega}$ ’s using marks 1) for 10^{-4} and 2) for 10^{-5} . The difference between the results for two $\bar{\omega}$ ’s is, however, much below any reasonable estimate of the theoretical accuracy.

The cross sections are shown in picobarn and the radiative corrections in percent. All the results in Tables 1 and 2 are derived in $\alpha(0)$ EW scheme and *after the subtraction of quark mass singularities in the \overline{MS} scheme*.

Each Table contains four rows of δ , two pairs for different $\bar{\omega}$ for $m_u = m_d = 0.066$ GeV and $m_u = m_d = 0.0066$ GeV. After subtraction of quark mass singularities the total cross section should be fully independent off quark masses. If cuts are applied, a residual depen-

dence arises, in principle, which becomes stronger if cuts get tighter. The numbers in the Tables 1 and 2 are derived for the only cut $M_{\mu^+\mu^-} \geq 50$ GeV. As seen, the residual quark mass dependence is very weak.

All the numbers were obtained with the aid of a FORTRAN code which consists of a hand-written `main` and FORTRAN modules automatically generated by `s2n.f` software of the SANC system, see Appendix.

4.1.2 $\alpha(0)$, G_F , G'_F schemes

Here we study the EW scheme dependence of the corrected cross section $\hat{\sigma}_1$ arising from the definition of EW constants in the $\alpha(0)$, G_F and G'_F schemes.

In Table 3 we show the results for $\hat{\sigma}_0$ and $\hat{\sigma}_1$ at the Born and one-loop levels and for the corresponding RC factors δ in three EW schemes.

The $\alpha(0)$ and G_F EW schemes are defined as usually [32]. In the G'_F scheme one assigns the same one-loop value of the coupling constant standing at all photon vertices $\alpha_{\text{QED}} \approx 1/132.544$. It has been adopted in Ref. [12] and used in Ref. [27] for the sake of comparison only.

The results for the radiative corrections are derived in \overline{MS} subtraction scheme, and the factorization scale is taken to be M_Z . There are notable deviations of the corrected cross sections from the corresponding Born values and between the Born values themselves in the three schemes. One can observe a certain degree of stabilization of one-loop corrected cross sections as

Table 1. The total lowest-order and one-loop corrected cross sections $\hat{\sigma}_0$ and $\hat{\sigma}_1$ for the process $u\bar{u} \rightarrow \mu^+\mu^-(\gamma)$ in the α EW scheme and corresponding relative one-loop correction δ for $\bar{\omega} = 10^{-4} \frac{\sqrt{s}}{2}$ GeV, rows 1) and $\bar{\omega} = 10^{-5} \frac{\sqrt{s}}{2}$ GeV, rows 2). Cut value: $M_{\mu^+\mu^-} \geq 50$ GeV.

\sqrt{s} , GeV	70	90	110	500	1000	2000	5000	14000
$\hat{\sigma}_0$, pb	4.312	369.6	4.995	7.324×10^{-2}	1.806×10^{-2}	4.499×10^{-3}	7.191×10^{-4}	9.171×10^{-5}
$\hat{\sigma}_1$, pb	4.713	397.2	4.732	8.403×10^{-2}	2.105×10^{-2}	5.256×10^{-3}	8.269×10^{-4}	1.010×10^{-4}
$m_q = m_u$								
δ , %, 1)	9.303	7.468	-5.259	14.74	16.61	16.84	14.99	10.09
δ , %, 2)	9.303	7.481	-5.261	14.74	16.61	16.84	14.99	10.09
$m_q = m_u/10$								
δ , %, 1)	9.296	7.466	-5.261	14.74	16.61	16.84	14.99	10.09
δ , %, 2)	9.296	7.480	-5.263	14.74	16.61	16.84	14.99	10.09

Table 2. The total lowest-order and one-loop corrected cross sections $\hat{\sigma}_0$ and $\hat{\sigma}_1$ for the process $d\bar{d} \rightarrow \mu^+\mu^-(\gamma)$ in the α EW scheme and corresponding relative one-loop correction δ for $\bar{\omega} = 10^{-4} \frac{\sqrt{s}}{2}$ GeV, rows 1) and $\bar{\omega} = 10^{-5} \frac{\sqrt{s}}{2}$ GeV, rows 2). Cut value: $M_{\mu^+\mu^-} \geq 50$ GeV.

\sqrt{s} , GeV	70	90	110	500	1000	2000	5000	14000
$\hat{\sigma}_0$, pb	2.895	472.9	5.237	3.968×10^{-2}	9.601×10^{-3}	2.381×10^{-3}	3.802×10^{-4}	4.847×10^{-5}
$\hat{\sigma}_1$, pb	3.079	497.3	5.318	4.439×10^{-2}	1.090×10^{-2}	2.692×10^{-3}	4.149×10^{-4}	4.863×10^{-5}
$m_q = m_d$								
δ , %, 1)	6.328	5.164	1.551	11.88	13.53	13.04	9.142	0.319
δ , %, 2)	6.327	5.167	1.550	11.88	13.53	13.04	9.141	0.317
$m_q = m_d/10$								
δ , %, 1)	6.329	5.162	1.552	11.88	13.53	13.04	9.142	0.318
δ , %, 2)	6.329	5.165	1.551	11.88	13.53	13.04	9.141	0.317

Table 3. The total lowest-order parton cross section $\hat{\sigma}_0$ and one-loop corrected cross section $\hat{\sigma}_1$ in pb and relative RC factor δ for the two EW schemes G_F and G'_F for $\bar{\omega} = 10^{-5} \frac{\sqrt{\hat{s}}}{2}$ GeV and invariant mass cut $M_{\mu^+\mu^-} = 50$ GeV; for details see the text.

$\sqrt{\hat{s}}$, GeV	70	90	110	500	1000	2000	5000	14000
$u\bar{u} \rightarrow \mu^+\mu^-(\gamma)$								
α								
Δ , %	-0.55	-1.41	-0.34	-0.59	-0.66	-0.64	-0.53	-0.30
G_F								
$\hat{\sigma}_0$, pb	4.434	394.9	5.259	7.464×10^{-2}	1.839×10^{-2}	4.581×10^{-3}	7.323×10^{-4}	9.338×10^{-5}
$\hat{\sigma}_1$, pb	4.739	402.9	4.748	8.453×10^{-2}	2.119×10^{-2}	5.290×10^{-3}	8.313×10^{-4}	1.013×10^{-4}
δ , %	6.878	2.019	-9.718	13.25	15.23	15.47	13.53	8.443
G'_F								
$\hat{\sigma}_0$, pb	4.608	395.0	5.338	7.826×10^{-2}	1.929×10^{-2}	4.807×10^{-3}	7.685×10^{-4}	9.800×10^{-5}
$\hat{\sigma}_1$, pb	4.805	403.2	4.759	8.657×10^{-2}	2.176×10^{-2}	5.442×10^{-3}	8.576×10^{-4}	1.048×10^{-4}
δ , %	4.285	2.075	-10.83	10.61	12.76	13.21	11.60	6.913
Δ , %	+1.01	+0.07	+0.23	+2.41	+2.69	+2.87	+3.16	+3.46
$d\bar{d} \rightarrow \mu^+\mu^-(\gamma)$								
α								
	-0.96	-1.29	-1.02	-1.06	-1.09	-1.07	-0.91	-0.045
G_F								
$\hat{\sigma}_0$, pb	3.055	505.3	5.573	4.144×10^{-2}	1.002×10^{-2}	2.485×10^{-3}	3.966×10^{-4}	5.057×10^{-5}
$\hat{\sigma}_1$, pb	3.109	503.8	5.373	4.487×10^{-2}	1.102×10^{-2}	2.721×10^{-3}	4.187×10^{-4}	4.885×10^{-5}
δ , %	1.781	-0.306	-3.593	8.268	9.994	9.509	5.550	-3.408
G'_F								
$\hat{\sigma}_0$, pb	3.094	505.3	5.596	4.240×10^{-2}	1.026×10^{-2}	2.545×10^{-3}	4.062×10^{-4}	5.180×10^{-5}
$\hat{\sigma}_1$, pb	3.126	503.7	5.371	4.534×10^{-2}	1.115×10^{-2}	2.756×10^{-3}	4.240×10^{-4}	4.940×10^{-5}
δ , %	1.026	-0.310	-4.027	6.932	8.718	8.291	4.368	-4.619
Δ , %	+0.55	-0.02	-0.04	+1.05	+1.18	+1.29	1.27	+1.13

can be seen from the rows of Δ values, showing deviations of $\hat{\sigma}_1$ in $\alpha(0)$ and G'_F schemes from $\hat{\sigma}_1$ in G_F scheme:

$$\Delta(\alpha, G'_F) = \hat{\sigma}_1(\alpha, G'_F)/\hat{\sigma}_1(G_F) - 1, \% . \quad (27)$$

However, for the process $u\bar{u} \rightarrow \mu^+\mu^-(\gamma)$, especially at high energies, the G'_F scheme does not seem to work satisfactorily.

Note, that for $\alpha(0)$ scheme it is sufficient to show only Δ -rows, since all the other entries are already given in Tables 1 and 2.

As concerning the choice between the $\alpha(0)$ and G_F schemes, we favor the latter since its effective energy scale is known to be of the order of a weak boson mass. Moreover, in the results presented in the $\alpha(0)$ scheme, the hadronic contribution to the vacuum polarization in the photon propagator is taken into account in an approximation, using the one-loop formulae supplied by the quark masses listed in Eq. (26). In any case the difference between the schemes is related to the contribution of higher orders of the perturbation theory and gives us a crude estimate of the corresponding contribution to the theoretical uncertainty.

4.2 Hadronic level

Results presented in this section were obtained with the aid of two standalone packages: 1) a MC integrator based on Vegas algorithm [33] and 2) a MC generator based on FOAM algorithm [30]. All the calculations are done with Les Houches 2005 setup [21] in G_F EW

scheme. Besides input parameters Eq. (26), one has to specify cuts on the lepton invariant mass $M_{\mu^+\mu^-}$, muons transverse momenta $p_T(\mu)$ and muons pseudorapidity $\eta(\mu)$ which were used at production of figures below:

$$\begin{aligned} M_{\mu^+\mu^-} &> 50\text{GeV}, \\ p_T(\mu^\pm) &> 25\text{GeV}, \\ |\eta(\mu^\pm)| &< 1.2. \end{aligned} \quad (28)$$

In Figs. 2 and 3 we show the distributions $d\sigma/dp_T$ and $d\delta/dp_T$ obtained with the aid of the MC integrator, while in the Figs. 4 and 5 the same distributions obtained with the aid of the generator. The corresponding distributions agree with each other within statistical errors, which are larger for the case of the MC event generator.

In the Figures 6 and 7 we show the distributions $d\sigma/dM$ and $d\delta/dM$ over invariant mass $M = M_{\mu^+\mu^-}$ for the case of the MC integrator, and in the Figures 8 and 9 — for the case of the generator.

One may draw the same conclusions as for the distributions in p_T .

The similar distributions are presented in Ref. [17] calculated, however, with different setup and cuts, therefore they cannot be compared straightforwardly.

5 Conclusions

In addition to the results presented here, one has to take into account one more $\mathcal{O}(\alpha)$ contribution of the

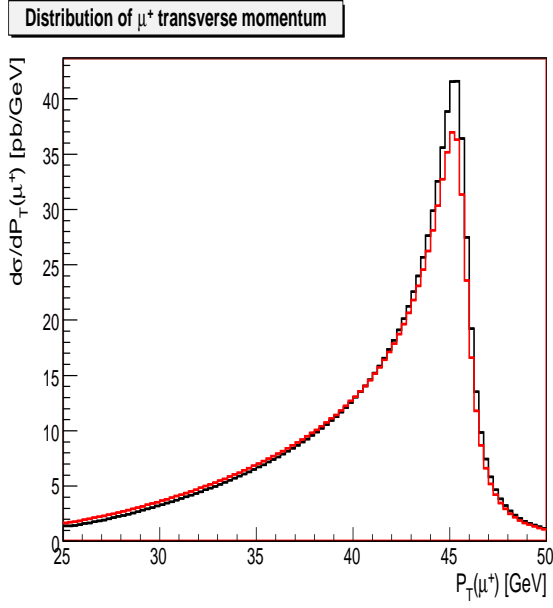


Fig. 2. Muon transverse momentum distribution for $\sqrt{s} = 14$ TeV, as obtained from the MC integrator. Both the Born (black line) and the one-loop results (red line) are shown.

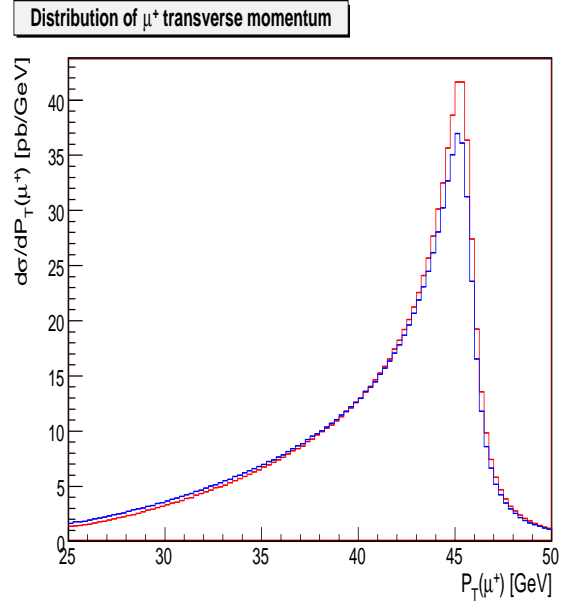


Fig. 4. Muon transverse momentum distribution for $\sqrt{s} = 14$ TeV, as obtained from the MC event generator. Both the Born (red line) and the one-loop results (blue line) are shown.

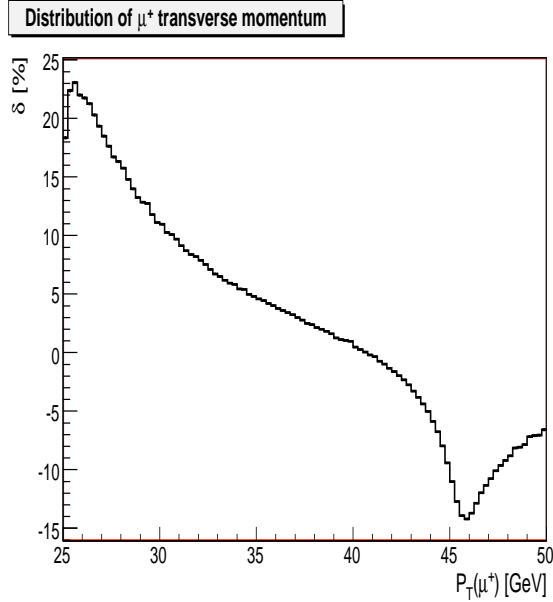


Fig. 3. Relative corrections δ as a function of the muon transverse momentum $p_T(\mu^+)$, as obtained from the MC integrator.

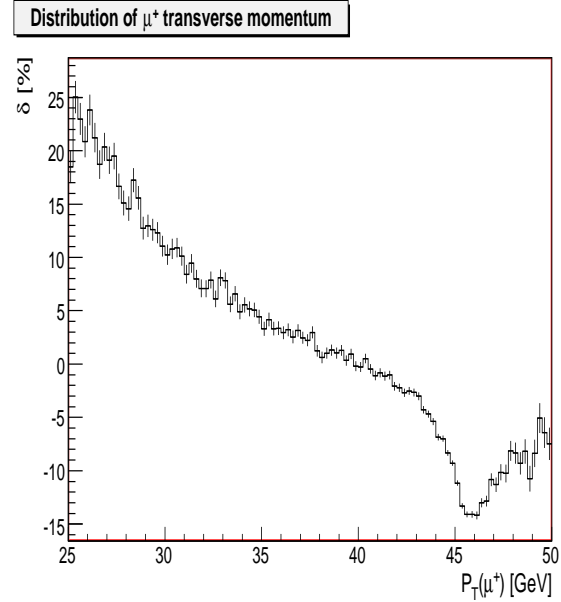


Fig. 5. Relative corrections δ as a function of the muon transverse momentum $p_T(\mu^+)$, as obtained from the MC event generator.

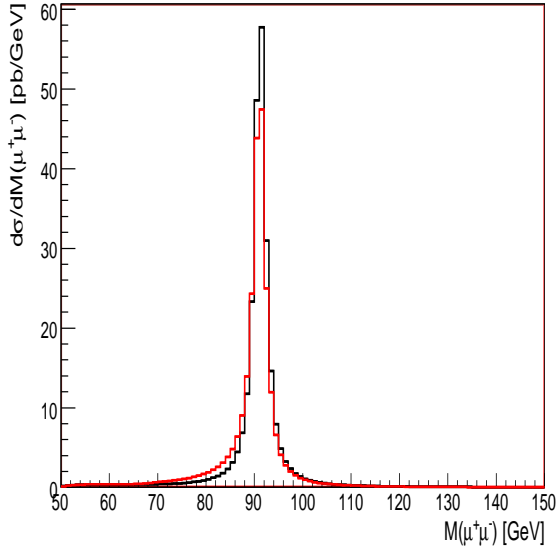
Distribution of invariant mass of $\mu^+\mu^-$ pair

Fig. 6. Invariant mass distribution of the $\mu^+\mu^-$ pair at $\sqrt{s} = 14$ TeV, as obtained from the MC integrator. Both the Born (black line) and the one-loop results (red line) are shown.

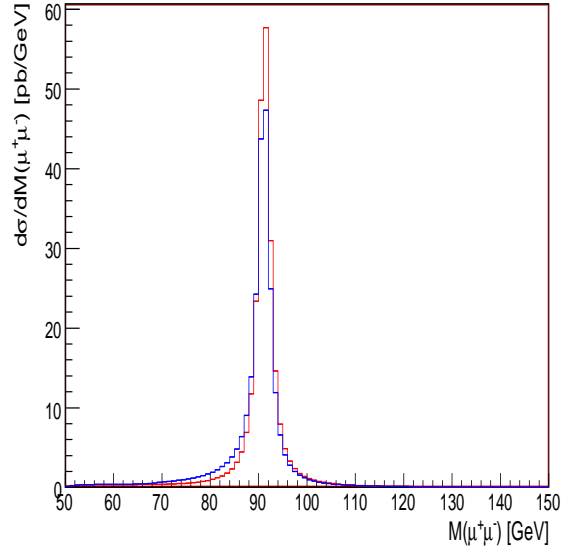
Distribution of invariant mass of $\mu^+\mu^-$ pair

Fig. 8. Invariant mass distribution of the $\mu^+\mu^-$ pair at $\sqrt{s} = 14$ TeV, as obtained from the MC event generator. Both the Born (red line) and the one-loop results (blue line) are shown.

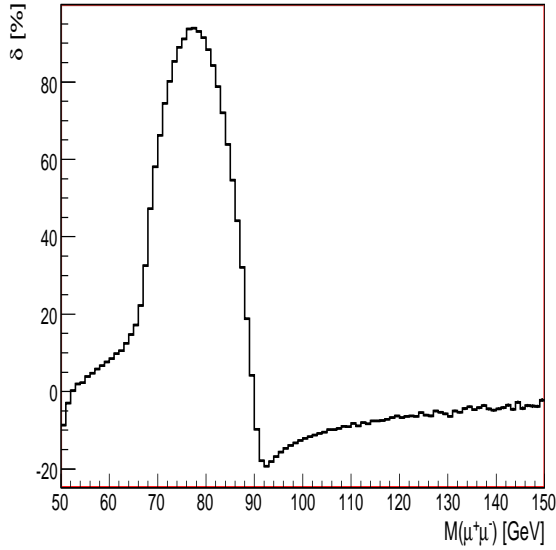
Distribution of invariant mass of $\mu^+\mu^-$ pair

Fig. 7. Relative corrections δ as a function of the invariant mass $M_{\mu^+\mu^-}$, as obtained from the MC integrator.

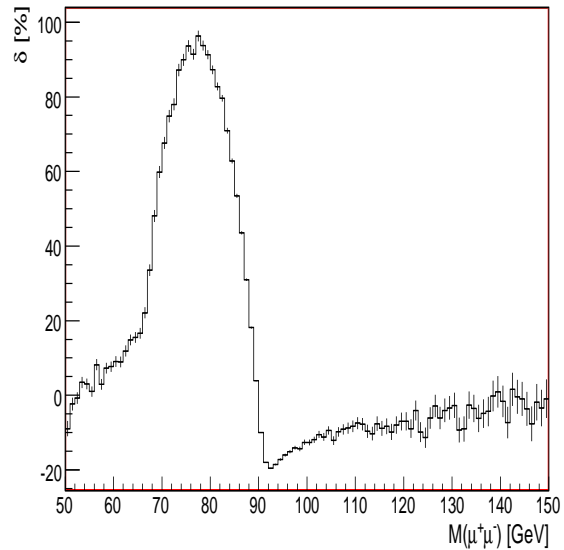
Distribution of invariant mass of $\mu^+\mu^-$ pair

Fig. 9. Relative corrections δ as a function of the invariant mass $M_{\mu^+\mu^-}$, as obtained from the MC event generator.

photon-induced subprocess $\gamma + q \rightarrow q + l + \bar{l}$, which was recently computed in Ref. [34].

In this way the complete set of one-loop electroweak radiative corrections to neutral current Drell–Yan pro-

cesses has been computed within the SANC system environment. Our results are implemented into semi-analytical FORTRAN codes as well as into a Monte Carlo event generator. The codes can help to increase an accuracy of the theoretical description of the SM processes, which is required for the forthcoming LHC data analysis. Tuned comparison of our results for NC DY with the ones of analogous calculations performed by other groups, started for the CC case in Refs. [21,22], is in progress within the Les Houches 2007 workshop. The comparison should help us to derive a common conclusion on the resulting theoretical uncertainty in our predictions.

Appendix

In the Appendix we present a Technical Description of the `sanc_dy_nc_v1.00` package intended for calculation of the total DY NC cross section at the partonic level.

The main aim of this description is to demonstrate how SANC Standard FORTRAN Modules (SSFM) can be used by other codes. We also give a short guide to the main flags which are being used not only in this package but also govern the work of any package which uses SSFM, as our integrators and generators do.

• Overview of the package

All files are produced by s2n package of SANC project (v.1.10) except `main*_xx.yy.F`, declaration files — `*.h` and libraries — `*.a`. Here “xx” and “yy” stand for the standard SANC field indices: 12 — e^- , 13 —

u , 14 — d , 16 — μ^- , etc. The package `sanc_dy_nc_v1.00` is accessible for the following set of particles: 1313_1212, 1313_1616, 1414_1212, 1414_1616.

Total set of files inside the package is:

Instruction files:

README
RELEASE-NOTES
CHANGES
LICENSE.TXT
INSTALL

Declaration files:

`s2n_declare.h`

Initialization and various input files:

`s2n_init.f`
`sanc_input.h`
`leshw_input.h`
`tev4lhwc_input.h`

Libraries for various functions, including Vegas integration, see INSTALL file in the package.

Main files: `main_nc_vegas_xx.yy.F`

SSFM originated from

<code>nc_ff_xx.yy.F</code>	(FF)
<code>nc_si_xx.yy.f</code>	(HA)
<code>nc_br_xx.yy.f</code>	(BR)

[this file contains three SSFM (subroutines)

<code>nc_bo_xx.yy (...)</code> , <code>nc_br_xx.yy (...)</code> , <code>nc_ha_xx_xx_1spr (...)</code>	
<code>nc_ha_xx.yy.f</code>	(MC)

The steps of calculation in the `main*` files in accordance with Eqs. (22), (18), (15) are:

- step of declaration and initialization
- step born is realized by flag `iborn=1`,
 $\hat{\sigma}_0$ is computed by integration over \hat{c} of Eq. (13) of the function_1c_xx_yy,
 - via SSFM call `nc_br_xx_yy (... ,born,...)`
- step $\hat{\sigma}_{SV}$ is realized by flag `iborn=0`,
 it is computed by integration over \hat{c} of the function_1c_xx_yy,
 - `virt` via SSFM call `nc_si_xx_yy (... ,sigma)` ,
 (inside this module there exists a call to SSFM `nc_ff_xx_yy (...)`)
 - `soft` via SSFM call `nc_br_xx_yy (... ,soft,...)`
- step $\Delta\hat{\sigma}_{SV}^{\overline{MS}}$
 by calculation of $\Delta\hat{\sigma}_{SV}^{\overline{MS}}$ through Eq.(19)
- step $\Delta\hat{\sigma}_{hard}^{\overline{MS}}$
 by integration over ξ of the function_1s_xx_yy
 - via SSFM call `nc_bo_xx_yy (... ,bornk)`,
 see Eq. (20)
- step $d\hat{\sigma}_{hard}/d\hat{s}'$
 by integration over \hat{s}' of the function_1spr_xx_yy
 - via SSFM call `nc_ha_xx_yy_1spr (... ,hard)`
 or alternatively
- step $d\sigma_{hard}/d\Phi^{(3)}$
 by integration over 4d-phase space of Eq. (6)–(7) of the function_4d_xx_yy
 - via SSFM call `nc_ha_xx_yy (... ,hard)`

• Options of the flags

iqed(I) – choice of calculations for QED correction:

- I=0 without QED correction
- I=1 with all QED correction
- I=2 with ISR QED correction
- I=3 with IFI QED correction
- I=4 with FSR QED correction

iew(I) – choice of calculations for EW correction:

- I=0 without EW correction
- I=1 with EW correction

iborn(I) – choice of scheme of calculations of the partonic cross section:

- I=1 only Born level
- I=0 Born + 1-loop virtual corrections

gfscheme(I) – choice of the EW scheme:

- I=0 $\alpha(0)$ scheme
- I=1 G_F scheme
- I=2 G'_F scheme

ilin(I) – choice of the linearization at the calculation of the partonic cross section:

- I=0 without linearization
- I=1 with linearization, *i.e.* neglecting spurious terms $\mathcal{O}(\alpha^2)$

ifgg(I) – choice of calculations of photonic vacuum polarization \mathcal{F}_{gg} :

- I=-1 — 0
- I= 0 — 1
- I= 1 — $1 + k\mathcal{F}_{gg}$
- I= 2 — $1/(1 - k\mathcal{F}_{gg})$

with $k = \frac{g^2}{16\pi^2}$.

ihard(I) – types of the hard bremsstrahlung phase-space integrations:

I=1 integration over \hat{s}'

I=4 4d integration

isetup(I) – choice of the setup:

I=0 Standard SANC

I=1 Les Houches Workshop

I=2 TeV4LHC Workshop

The package can be accessed from project home-pages http://pcphysanc.cern.ch/download/sanc_dy_nc_v1.00.tgz or http://sanc.jinr.ru/download/sanc_dy_nc_v1.00.tgz.

Acknowledgment

We are grateful to V. Kolesnikov, E. Uglov and V. Zykunov for discussions.

This work is partly supported by INTAS grant N° 03-51-4007, by the EU grant mTkd-CT-2004-510126 in partnership with the CERN Physics Department and by the Polish Ministry of Scientific Research and Information Technology grant No 620/E-77/6.PRUE/DIE 188/2005-2008 and by Russian Foundation for Basic Research grant N° 07-02-00932. One of us (A.A.) thanks also the grant of the President RF Scientific Schools 5332.2006.

References

1. S. D. Drell and T.-M. Yan, *Phys. Rev. Lett.* **25** (1970) 316–320.
2. U. Baur, *Submitted to Int.J.Mod.Phys.E* (2007) [hep-ph/0701164](#).
3. C. M. Carloni Calame, G. Montagna, O. Nicrosini, F. Piccinini, and A. Vicini, *AIP Conf. Proc.* **870** (2006) 436–439.
4. M. Dittmar, F. Pauss, and D. Zurcher, *Phys. Rev.* **D56** (1997) 7284–7290, [hep-ex/9705004](#).
5. S. Frixione and M. L. Mangano, *JHEP* **05** (2004) 056, [hep-ph/0405130](#).
6. CDF Collaboration, V. M. Abazov *et al.*, *Phys. Rev.* **D70** (2004) 092008, [hep-ex/0311039](#).
7. CDF Collaboration, A. Abulencia *et al.*, [hep-ex/0508029](#).
8. V. A. Mosolov and N. M. Shumeiko, *Nucl. Phys.* **B186** (1981) 397–411.
9. A. V. Soroko and N. M. Shumeiko, *Sov. J. Nucl. Phys.* **52** (1990) 329–334.
10. D. Wackeroth and W. Hollik, *Phys. Rev.* **D55** (1997) 6788–6818, [hep-ph/9606398](#).
11. U. Baur, S. Keller, and D. Wackeroth, *Phys. Rev.* **D59** (1999) 013002, [hep-ph/9807417](#).
12. S. Dittmaier and M. Kramer, *Phys. Rev.* **D65** (2002) 073007, [hep-ph/0109062](#).
13. U. Baur, O. Brein, W. Hollik, C. Schappacher, and D. Wackeroth, *Phys. Rev.* **D65** (2002) 033007, [hep-ph/0108274](#).
14. U. Baur and D. Wackeroth, *Nucl. Phys. Proc. Suppl.* **116** (2003) 159–163, [hep-ph/0211089](#).
15. U. Baur and D. Wackeroth, *Phys. Rev.* **D70** (2004) 073015, [hep-ph/0405191](#).
16. C. M. Carloni Calame, G. Montagna, O. Nicrosini, and A. Vicini, *JHEP* **12** (2006) 016, [hep-ph/0609170](#).

17. C. M. Carloni Calame, G. Montagna, O. Nicrosini and A. Vicini, *JHEP* **10** (2007) 109, [arXiv:0710.1722](https://arxiv.org/abs/0710.1722) [[hep-ph](#)]
18. R. Hamberg, W. L. van Neerven, and T. Matsuura, *Nucl. Phys.* **B359** (1991) 343–405.
19. C. Anastasiou, L. J. Dixon, K. Melnikov, and F. Petriello, *Phys. Rev.* **D69** (2004) 094008, [hep-ph/0312266](#).
20. K. Melnikov and F. Petriello, *Phys. Rev.* **D74** (2006) 114017, [hep-ph/0609070](#).
21. C. Buttar *et al.*, [hep-ph/0604120](#).
22. TeV4LHC-Top and Electroweak Working Group Collaboration, C. E. Gerber *et al.*, [arXiv:0705.3251](#) [[hep-ph](#)].
23. A. Andonov *et al.*, *Comput. Phys. Commun.* **174** (2006) 481–517, [hep-ph/0411186](#). Erratum-ibid **177** (2007) 623–624.
24. D. Bardin *et al.*, *Comput. Phys. Commun.* DOI [10.1016/j.cpc.2007.06.006](#), [hep-ph/0506120](#).
25. C. M. Carloni Calame, G. Montagna, O. Nicrosini, and M. Treccani, *JHEP* **05** (2005) 019, [hep-ph/0502218](#).
26. V. A. Zykunov, *Phys. Rev.* **D75** (2007) 073019, [hep-ph/0509315](#).
27. A. Arbuzov *et al.*, *Eur. Phys. J.* **C46** (2006) 407–412, [hep-ph/0506110](#). Erratum-ibid **C50** (2007) 505.
28. V. Kolesnikov, *talk to ATLAS MC, CERN* (12, 2006) <http://indico.cern.ch/conferenceDisplay.py?confId=6818>.
29. A. Andonov *et al.*, *Physics of Particles and Nuclei Letters* **4** (2007) 451–460, [hep-ph/0610268](#).
30. S. Jadach and P. Sawicki, *Comput. Phys. Commun.* **177** (2007) 441–458, [physics/0506084](#).
31. R. Sadykov, *talk at ATLAS, CERN* (10, 2007) <http://indico.cern.ch/conferenceDisplay.py?confId=10887>.
32. W. Hollik and H. J. Timme, *Z. Phys.* **C33** (1986) 125.
33. G. P. Lepage, *J. Comput. Phys.* **27** (1978) 192.
34. A. B. Arbuzov and R. R. Sadykov, [arXiv:0707.0423](#) [[hep-ph](#)].